AIMS Mathematics, 7(12): 20962–20978.
DOI:10.3934/math.20221148
Received: 26 July 2022
Revised: 10 December 2022
Accepted: 19 December 2022
Published: 27 December 2022

http://www.aimspress.com/journal/Math

Research article

A posteriori grid method for a time-fractional Black-Scholes equation

Zhongdi Cen, Jian Huang* and Aimin Xu

Institute of Mathematics, Zhejiang Wanli University, Ningbo 315100, China

* **Correspondence:** Email: sword@zwu.edu.cn.

Abstract: In this paper, a posteriori grid method for solving a time-fractional Black-Scholes equation governing European options is studied. The possible singularity of the exact solution complicates the construction of the discretization scheme for the time-fractional Black-Scholes equation. The $L1$ method on an arbitrary grid is used to discretize the time-fractional derivative and the central difference method on a piecewise uniform grid is used to discretize the spatial derivatives. Stability properties and a posteriori error analysis for the discrete scheme are studied. Then, an adapted a posteriori grid is constructed by using a grid generation algorithm based on a posteriori error analysis. Numerical experiments show that the $L1$ method on an adapted a posteriori grid is more accurate than the method on the uniform grid.

Keywords: option valuation; Black-Scholes equation; fractional differential equation; a posteriori grid; a posteriori error analysis
Mathematics Subject Classification: 65M06, 65M12, 65M15

1. Introduction

The classical Black-Scholes model was widely used in pricing options [3, 23]. However, the classical Black-Scholes model is established under ideal assumptions which are not entirely consistent with the real stock movement. Along with the discovery of the fractional structure of the stochastic processes, fractional option pricing models have attracted more and more attention from academia and the securities industry. Various types of fractional option pricing models have been derived, see [4,8,11,17,24,32,34] for example. The following time-fractional Black-Schole equation (TFBSE) developed by Wyss [34] is one of the most commonly used models:

$$\begin{cases} \frac{\partial^\alpha u}{\partial t^\alpha} - \frac{1}{2}\sigma^2 x^2 \frac{\partial^2 u}{\partial x^2} - (r-q)\, x \frac{\partial u}{\partial x} + ru = 0, & (x,t) \in \mathbb{R}^+ \times (0,T], \\ u(x,0) = \max(x-E,0), & x > 0, \\ u(0,t) = 0, & t \in [0,T], \end{cases} \tag{1.1}$$

where $u(x,t)$ is the European option price at asset price x and time $T-t$, T is the maturity time, σ is the volatility of the asset price, r is the risk-free interest rate, q is the continuous dividend rate, E is the exercise price, $\frac{\partial^\alpha u}{\partial t^\alpha}$ is the α-order Caputo fractional derivative defined as

$$\frac{\partial^\alpha u}{\partial t^\alpha} = \frac{1}{\Gamma(1-\alpha)} \int_0^t (t-s)^{-\alpha} \frac{\partial u}{\partial t}(x,s)\mathrm{d}s, \qquad 0 < \alpha < 1.$$

Compared to the classical Black-Scholes model, the time-fractional Black-Scholes model can better grasp both major jumps over small time periods and long-range dependencies in markets [27].

The fractional differential equations often need to be solved numerically due to the unavailability of analytical solutions. Some literatures have studied the numerical solutions of TFBSEs. The implicit finite difference methods for the TFBSE have been developed by Song and Wang [28] and Zhang et al. [35, 36]. A weighted finite difference scheme for the FEBSE of Jumarie type has been proposed by Koleva and Vulkov [18]. A compact finite difference method is described by Roul and Goura [26] for solving the FEBSE. Higher order convergence schemes have been derived by De Staelen and Hendy [29] and Abdi et al. [1]. A finite difference method along with a radial basis functions method and the moving least-squares approach also have been described by Golbabai et al. [12, 13] for solving the FEBSEs. The residual power series method along with the mesh-free collocation method has been used to solve the FEBSEs by Haq and Hussain [15]. A compact quadratic spline collocation method for the TFBSE is derived by Tian et al. [32]. An operator splitting method is used to solve the American-type FEBSE by Chen et al. [7]. A numerical method based on the extension of a Crank-Nicolson method is also applied to the FEBSE by Nuugulu et al. [24]. A space-time spectral method is proposed by An et al. [2] for solving the FEBSE. However, the above literatures imply the assumption that the exact solutions of the FEBSEs are sufficiently smooth.

In fact, the exact solutions of the fractional differential equations often have singularities, see [25,30, 31] and the references therein. The adapted grid method is often used to deal with the singular behavior of the exact solutions. There are two types of adapted grids: a priori grids and a posteriori grids. The construction of a priori grids needs a priori information about the exact solutions. She et al. [27] showed the solution of the FEBSE has an initial layer and used a modified $L1$ time discretization based on a change of variable to solve it. Cen et al. [5] developed a discrete scheme on a priori grid for the FEBSE by using a priori information about the exact solution. Huang et al. [16] also presented an adaptive moving grid based on a priori error analysis for the FEBSE. However, a priori information of the exact solution is often not easy to obtain, while the construction of a posteriori grid does not need to know a priori information of the exact solution, so a posteriori grid method has a wider application (see, e.g., [9, 20, 21]).

In this paper an adapted a posteriori grid method for solving the TFBSE (1.1) is considered. We discretize the time-fractional derivative by using the $L1$ approximation method on an arbitrary grid and discretize the spatial derivatives by using the central difference method on a piecewise uniform grid. We give a proof of the stability of the spatial semi-discrete operator and derive a posteriori error analysis for the discrete scheme. Then, we construct an adapted a posteriori grid for the time discretization by equidistributing a modified arc-length monitor function based on a posteriori error analysis. Finally, it can be seen from the numerical experiments that a posteriori-adapted grid fits the singularity of the exact solution well and the $L1$ method with a posteriori-adapted grid is more accurate than the method on the uniform grid. The contribution of this paper is to apply a posteriori grid method to solve the FEBSEs for the first time, which does not need a priori information of the exact solution.

The structure of the rest of the paper is as follows. The discretization method is introduced in Section 2. A posteriori error analysis for the scheme is derived in Section 3. A posteriori solution-adapted algorithm is established in Section 4. Numerical results are presented in Section 5. Conclusions and discussion are given in the last section.

Notation. In this paper, C is a positive constant independent of the grid, and C can denote different values in different places. For any function φ defined on the defined domain, let's make $\varphi_i^j = \varphi(x_i, t_j)$ to simplify the notation. The (pointwise) maximum norm on the defined domain is defined by $\|\cdot\|$.

2. Discretization

For numerical calculation, the infinite domain $\mathbb{R}^+\times(0,T]$ should be truncated into $\Omega = (0,X)\times(0,T]$ with $X = 4E$, where we have used the estimate of Willmott et al. [33]. Then, the right boundary condition can be obtained $u(X,t) = X - Ee^{-rt}$ according to the properties of the European option. Generally, the error caused by the truncation of the infinite domain can be ignored. Hence, the pricing model (1.1) can be reduced to the following fractional differential equation:

$$\begin{cases} Lu(x,t) \equiv \frac{\partial^\alpha u}{\partial t^\alpha} - \frac{1}{2}\sigma^2 x^2 \frac{\partial^2 u}{\partial x^2} - (r-q)\, x\frac{\partial u}{\partial x} + ru = 0, & (x,t) \in \Omega, \\ u(x,0) = \max(x-E,0), & x \in [0,X], \\ u(0,t) = 0, \quad u(x,t) = X - Ee^{-rt}, & t \in [0,T]. \end{cases} \tag{2.1}$$

First we give the spatial discretization scheme for problem (2.1). We employ a uniform grid

$$\Omega^N = \{x_i = ih \,|\, 0 \le i \le N,\ h = X/N\}$$

on $[0,X]$ with N grid elements when $\sigma^2 \ge |r-q|$. When $\sigma^2 < |r-q|$ the fractional Black-Scholes differential operator L is convection-dominated near $x = 0$. Therefore, in order to ensure the stability of the discrete scheme by using the central difference method for discretizing the spatial derivatives, we construct the following piecewise uniform grid

$$\bar{\Omega}^N = \{x_i \,|\, 0 \le i \le N\}$$

when $\sigma^2 < |r-q|$ as that in [6] with

$$x_i = \begin{cases} ih, & i = 0,1, \\ h\left[1 + \frac{\sigma^2}{|r-q|}(i-1)\right], & i = 2,3,\cdots,N, \end{cases} \tag{2.2}$$

where

$$h = \frac{X}{1 + \frac{\sigma^2}{|r-q|}(N-1)}.$$

Moreover, $h_i = x_i - x_{i-1}$ for $1 \le i \le N$ denote the spatial grid widths.

Thus, for each t we employ a central difference scheme on Ω^N to discrete the spatial derivatives:

$$\frac{\partial^\alpha U_i}{\partial t^\alpha} - \frac{\sigma^2 x_i^2}{h_i + h_{i+1}}\left(\frac{U_{i+1}(t) - U_i(t)}{h_{i+1}} - \frac{U_i(t) - U_{i-1}(t)}{h_i}\right)$$

$$
\begin{aligned}
&-(r-q)\,x_i\frac{U_{i+1}(t)-U_{i-1}(t)}{h_i+h_{i+1}}+rU_i(t)=0, \qquad 1\le i<N,\\
&U_0(t)=0, \quad U_N(t)=X-Ee^{-rt}.
\end{aligned}
$$

This discretization leads to an initial value problem of the form

$$
\begin{cases} L^N\mathbf{U}(t)\equiv\frac{\partial^\alpha\mathbf{U}}{\partial t^\alpha}+\mathbf{A}(t)\mathbf{U}(t)=\mathbf{f}(t),\\ \mathbf{U}(0)=\mathbf{g}, \end{cases} \tag{2.3}
$$

where $\mathbf{U}(t)=(U_1(t),\ldots,U_{N-1}(t))^T$, $\mathbf{A}(t)$ is a $(N-1)\times(N-1)$ matrix given by

$$
\mathbf{A}(t)=\begin{bmatrix}
b_1 & c_1 & & \cdots & & & 0\\
a_2 & b_2 & c_2 & \cdots & & & \vdots\\
\vdots & a_3 & b_3 & c_3 & \cdots & & \\
 & \vdots & \vdots & \vdots & \vdots & \vdots & \\
 & & & \cdots & a_{N-2} & b_{N-2} & c_{N-2}\\
0 & \cdots & & & & a_{N-1} & b_{N-1}
\end{bmatrix}
$$

with

$$
\begin{aligned}
&a_i=-\frac{\sigma^2x_i^2}{(h_i+h_{i+1})h_i}+\frac{(r-q)\,x_i}{h_i+h_{i+1}}, \quad b_i=\frac{\sigma^2x_i^2}{h_ih_{i+1}}+r,\\
&c_i=-\frac{\sigma^2x_i^2}{(h_i+h_{i+1})h_{i+1}}-\frac{(r-q)\,x_i}{h_i+h_{i+1}} \qquad \text{for } i=1,\cdots,N-1.
\end{aligned}
$$

The vectors $\mathbf{f}(t)$ and $\mathbf{g}$ are the corresponding boundary and initial conditions:

$$
\mathbf{f}(t)=\begin{pmatrix} -a_1U_0(t)\\ 0\\ \vdots\\ 0\\ -c_{N-1}U_N(t)\end{pmatrix}, \qquad \mathbf{g}=\begin{pmatrix} \max(x_1-E,0)\\ \max(x_2-E,0)\\ \vdots\\ \max(x_{N-1}-E,0)\end{pmatrix}.
$$

It is easy to know that the matrix $\mathbf{A}(t)$ is strictly diagonally dominant by simple calculation, which will be used in proving the semi-discrete maximum principle.

Next, on the time domain $[0,T]$ we introduce an arbitrary grid $\Omega^K\equiv\{0=t_0<t_1<\cdots<t_K=T\}$, where the time grid width is denoted by $\Delta t_j=t_j-t_{j-1}$ for $1\le j\le K$. We use the $L1$ approximation method [31] to discrete the time-fractional derivative

$$
\begin{aligned}
\frac{\partial^\alpha U_i}{\partial t^\alpha}(t_j) &= \frac{1}{\Gamma(1-\alpha)}\sum_{k=1}^{j}\int_{t_{k-1}}^{t_k}\left(t_j-s\right)^{-\alpha}U_i'(s)\,\mathrm{d}s\\
&\approx \frac{1}{\Gamma(1-\alpha)}\sum_{k=1}^{j}\int_{t_{k-1}}^{t_k}\left(t_j-s\right)^{-\alpha}D_t^-U_i^k\mathrm{d}s,
\end{aligned}
$$

where $D_t^- U_i^k = \frac{U_i^k - U_i^{k-1}}{\Delta t_k}$. Thus, combining the spatial discretization scheme and the time discretization scheme, we get the following fully discretization scheme for problem (2.1)

$$\begin{cases} \dfrac{1}{\Gamma(2-\alpha)} \displaystyle\sum_{k=1}^{j} \left[\left(t_j - t_{k-1}\right)^{1-\alpha} - \left(t_j - t_k\right)^{1-\alpha} \right] D_t^- \mathbf{U}^k + \mathbf{A}(t_j)\mathbf{U}^j = \mathbf{f}^j, \\ \mathbf{U}^0 = \mathbf{g}, \end{cases} \tag{2.4}$$

where $\mathbf{U}^j = \left(U_1^j, \ldots, U_{N-1}^j\right)^T$ and $\mathbf{f}^j = \left(f_1^j, \ldots, f_{N-1}^j\right)^T$.

3. A posteriori error analysis

In order to carry out a posteriori error analysis, we present a stability result for the fractional differential operator L^N. First we introduce a function space $W^1((0,T])$, which represents the space of functions $p(t) \in C^1((0,T])$ so that $p'(t)$ has Lebesgue integrability in $(0,T]$. Then we further introduce the following result for the Caputo derivative as Theorem 1 of [22].

Lemma 3.1. Suppose $w(t) \in W^1((0,T]) \cap C([0,T])$ reaches its minimum at the point $t^* \in (0,T]$, then $\frac{d^\alpha w}{dt^\alpha}(t^*) \leq 0$ for $0 < \alpha < 1$.

Thus the following semi-discrete maximum principle for L^N can be proved by using Lemma 3.1.

Lemma 3.2. (Semi-discrete maximum principle) Let $\mathbf{z}(t) = (z_1(t), \ldots, z_{N-1}(t))^T$ and $z_i(t) \in W^1((0,T]) \cap C([0,T])$ for $1 \leq i < N$. If $L^N \mathbf{z}(t) \geq \mathbf{0}$ for $t \in (0,T)$ with $\mathbf{z}(0) \geq \mathbf{0}$, then $\mathbf{z}(t) \geq \mathbf{0}$ for all $t \in [0,T]$.

Proof. We give the proof by contradiction. Assume that there exist i^*, t^* such that $z_{i^*}(t^*) = \min\limits_{i,t} z_i(t) < 0$. From the hypotheses of the lemma, we have $t^* \neq 0$. Thus, by applying Lemma 3.1 and the results $a_i \leq 0, c_i \leq 0$ and $a_i + b_i + c_i > 0$ we can get

$$\begin{aligned} L^N \mathbf{z}_{i^*}(t^*) &= \frac{d^\alpha z_{i^*}}{dt^\alpha}(t^*) + a_{i^*} z_{i^*-1}(t^*) + b_{i^*} z_{i^*}(t^*) + c_{i^*} z_{i^*+1}(t^*) \\ &\leq \frac{d^\alpha z_{i^*}}{dt^\alpha}(t^*) + \left(a_{i^*} + b_{i^*} + c_{i^*}\right) z_{i^*}(t^*) < 0, \end{aligned}$$

which contradicts the hypotheses of the lemma. Therefore, the original assumption is false and the minimum of z is non-negative. □

Then the following semi-discrete stability result for L^N can be obtained by using the semi-discrete maximum principle in Lemma 3.2.

Lemma 3.3. (Semi-discrete stability result) For any function vector $\mathbf{z}(t) \in W^1((0,T]) \cap C([0,T])$ we have the following estimate

$$\|\mathbf{z}(t)\|_{[0,T]} \leq \max\left\{ \|\mathbf{z}(0)\|, \max_{1 \leq i \leq N-2} \left\|L^N z_i(t)\right\|_{[0,T]}, \frac{4h_N^2}{\sigma^2 x_{N-1}^2} \left\|L^N z_{N-1}(t)\right\|_{[0,T]} \right\}$$

with sufficiently large N.

Applying the above semi-discrete stability result and the truncation error estimates of the spatial discrete scheme, we have the following error estimates.

Theorem 3.4. Let $u(x,t)$ and $\mathbf{U}(t)$ be the solutions of problems (2.1) and (2.3) respectively. Then, under the assumptions [5, 16]

$$\left|x^2\frac{\partial^4 u}{\partial x^4}\right| \le C, \quad \left|x\frac{\partial^3 u}{\partial x^3}\right| \le C, \tag{3.1}$$

the following error estimates

$$\|u(x_i,t) - U_i(t)\|_{[0,T]} \le CN^{-2} \tag{3.2}$$

for $0 \le i \le N$ hold true, where C is a positive constant independent of the grid.

Proof. The following truncation error estimates can be obtained by using Taylor expansions about $x = x_i$

$$\begin{aligned}\left|L^N\left(u(x_i,t) - U_i(t)\right)\right| &\le C\left(h_i + h_{i+1}\right)\int_{x_{i-1}}^{x_{i+1}}\left[x_i^2\left|\frac{\partial^4 u}{\partial x^4}(x,t)\right| + x_i\left|\frac{\partial^3 u}{\partial x^3}(x,t)\right|\right]\mathrm{d}x\\ &\le CN^{-2}\end{aligned}$$

for $1 \le i < N$, where the spatial grid widths and the assumptions (3.1) have been used. Furthermore, it is easy to see that $u(x_i,t) \in W^1((0,T]) \cap C([0,T])$ for each i. Thus, the desired results of the lemma can be get by applying Lemma 3.3. □

Next, a posteriori error analysis for the numerical method (2.4) will be derived. Suppose $\bar{U}_i^K(t)$ is a piecewise linear interpolant function of the numerical solution $\left\{U_i^j\right\}_{j=0}^K$ for each i, then $\bar{U}_i^K(t)$ is continuous on $[0,T]$, linear on each $[t_{j-1},t_j]$ and

$$\bar{U}_i^K(t_j) = U_i^j, \qquad 0 \le j \le K. \tag{3.3}$$

Furthermore, suppose $\bar{\mathbf{U}}^K(t) = \left(\bar{U}_1^K(t), \bar{U}_2^K(t), \ldots, \bar{U}_{N-1}^K(t)\right)^T$ denotes a piecewise linear interpolant function vector.

Theorem 3.5. Let $\mathbf{U}(t)$ be the solution vector of the semi-discrete problem (2.3), $\left\{\mathbf{U}^j\right\}_{j=0}^K$ be the numerical solution vector of the fully discrete problem (2.4) and $\bar{\mathbf{U}}^K(t)$ be its piecewise linear interpolant function vector. Then the following estimate

$$\left\|\bar{\mathbf{U}}^K(t) - \mathbf{U}(t)\right\|_{[0,T]} \le C \max_{1\le i\le N, 1\le j\le K}\left\{\left(\triangle t_j\right)^2 + \left(\triangle t_j\right)^{1-\alpha}\left|D_t^- U_i^j\right|\right\} \tag{3.4}$$

holds true.

Proof. By the definition of $\bar{\mathbf{U}}^K(t)$ we know

$$\bar{\mathbf{U}}^K(t) = \mathbf{U}^j + \left(t - t_j\right)D_t^-\mathbf{U}^j \quad \text{and} \quad \frac{d\bar{\mathbf{U}}^K}{dt} = D_t^-\mathbf{U}^j \quad \text{for } t \in (t_{j-1},t_j). \tag{3.5}$$

For $t \in (t_{j-1},t_j)$ we have the following derivation

$$L^N\left(\bar{U}_i^K(t) - U_i(t)\right) = \frac{1}{\Gamma(1-\alpha)}\sum_{k=1}^{j-1}\int_{t_{k-1}}^{t_k}(t-s)^{-\alpha}\frac{d\bar{U}_i^K(s)}{ds}\mathrm{d}s$$

$$
\begin{aligned}
&+\frac{1}{\Gamma(1-\alpha)}\int_{t_{j-1}}^{t}(t-s)^{-\alpha}\frac{d\bar{U}_i^K(s)}{ds}\mathrm{d}s + a_i\bar{U}_{i-1}^K(t) + b_i\bar{U}_i^K(t) + c_i\bar{U}_{i+1}^K(t) - f_i(t)\\
&= \frac{1}{\Gamma(1-\alpha)}\sum_{k=1}^{j-1}\int_{t_{k-1}}^{t_k}(t-s)^{-\alpha}D_t^- U_i^k\mathrm{d}s + \frac{1}{\Gamma(1-\alpha)}\int_{t_{j-1}}^{t}(t-s)^{-\alpha}D_t^- U_i^j\mathrm{d}s\\
&\quad +a_i\bar{U}_{i-1}^K(t) + b_i\bar{U}_i^K(t) + c_i\bar{U}_{i+1}^K(t) - \bar{f}_i(t) + \left(\bar{f}_i(t) - f_i(t)\right)\\
&= \frac{1}{\Gamma(2-\alpha)}\sum_{k=1}^{j-1}\left[(t-t_{k-1})^{1-\alpha} - (t-t_k)^{1-\alpha}\right]D_t^- U_i^k + \frac{\left(t-t_{j-1}\right)^{1-\alpha}}{\Gamma(2-\alpha)}D_t^- U_i^j\\
&\quad +a_i\left[U_{i-1}^j + \left(t-t_j\right)D_t^- U_{i-1}^j\right] + b_i\left[U_i^j + \left(t-t_j\right)D_t^- U_i^j\right]\\
&\quad +c_i\left[U_{i+1}^j + \left(t-t_j\right)D_t^- U_{i+1}^j\right] - \left[f_i^j + \left(t-t_j\right)D_t^- f_i^j\right] + \left(\bar{f}_i(t) - f_i(t)\right)\\
&= \frac{1}{\Gamma(2-\alpha)}\sum_{k=1}^{j-1}\left[(t-t_{k-1})^{1-\alpha} - (t-t_k)^{1-\alpha}\right]D_t^- U_i^k + \frac{\left(t-t_{j-1}\right)^{1-\alpha}}{\Gamma(2-\alpha)}D_t^- U_i^j\\
&\quad -\frac{1}{\Gamma(2-\alpha)}\sum_{k=1}^{j}\left[\left(t_j-t_{k-1}\right)^{1-\alpha} - \left(t_j-t_k\right)^{1-\alpha}\right]D_t^- U_i^k + \left(\bar{f}_i(t) - f_i(t)\right)\\
&\quad +\left(t-t_j\right)\left(a_iD_t^- U_{i-1}^j + b_iD_t^- U_i^j + c_iD_t^- U_{i+1}^j - D_t^- f_i^j\right),
\end{aligned}
\tag{3.6}
$$

where (2.4), (3.5) and $\bar{f}_i(t) = f_i^j + \left(t-t_j\right)D_t^- f_i^j$ for $t \in (t_{j-1}, t_j)$ have been used.

By using the mean value theorem we have

$$
\begin{aligned}
&\left|\frac{1}{\Gamma(2-\alpha)}\sum_{k=1}^{j-1}\left[(t-t_{k-1})^{1-\alpha} - (t-t_k)^{1-\alpha}\right]D_t^- U_i^k + \frac{1}{\Gamma(2-\alpha)}\left(t-t_{j-1}\right)^{1-\alpha}D_t^- U_i^j\right.\\
&\quad \left.-\frac{1}{\Gamma(2-\alpha)}\sum_{k=1}^{j}\left[\left(t_j-t_{k-1}\right)^{1-\alpha} - \left(t_j-t_k\right)^{1-\alpha}\right]D_t^- U_i^k\right|\\
&\le \left|\frac{1}{\Gamma(2-\alpha)}\sum_{k=1}^{j-1}\left\{\left[(t-t_{k-1})^{1-\alpha} - (t-t_k)^{1-\alpha}\right] - \left[\left(t_j-t_{k-1}\right)^{1-\alpha} - \left(t_j-t_k\right)^{1-\alpha}\right]\right\}D_t^- U_i^k\right|\\
&\quad +\left|\frac{1}{\Gamma(2-\alpha)}\left[\left(t-t_{j-1}\right)^{1-\alpha} - \left(t_j-t_{j-1}\right)^{1-\alpha}\right]D_t^- U_i^j\right|\\
&\le \frac{1}{\Gamma(1-\alpha)}\left|\sum_{k=1}^{j-1}\left[\left(\xi_j-t_{k-1}\right)^{-\alpha} - \left(\xi_j-t_k\right)^{-\alpha}\right](t_j-t)D_t^- U_i^k\right| + \frac{\left(\triangle t_j\right)^{1-\alpha}}{\Gamma(2-\alpha)}\left|D_t^- U_i^j\right|\\
&\le \frac{\alpha}{\Gamma(1-\alpha)}\left|\sum_{k=1}^{j-1}\left(\xi_j-\nu_k\right)^{-\alpha-1}(t_j-t)\triangle t_kD_t^- U_i^k\right| + \frac{\left(\triangle t_j\right)^{1-\alpha}}{\Gamma(2-\alpha)}\left|D_t^- U_i^j\right|\\
&\le C\max_{1\le k\le j}(\triangle t_k)^{1-\alpha}\left|D_t^- U_i^k\right|,
\end{aligned}
\tag{3.7}
$$

where $\xi_j \in (t, t_j)$ and $\nu_k \in (t_{k-1}, t_k)$. By using the discrete equation (2.4) and the mean value theorem we also can obtain

$$
\left|\left(t-t_j\right)\left(a_iD_t^- U_{i-1}^j + b_iD_t^- U_i^j + c_iD_t^- U_{i+1}^j - D_t^- f_i^j\right)\right|
$$

$$
\begin{aligned}
&= \left|\left(t-t_j\right) D_t^- \left(a_i U_{i-1}^j + b_i U_i^j + c_i U_{i+1}^j - f_i^j\right)\right| \\
&\le \frac{t_j - t}{\Gamma(2-\alpha)\triangle t_j} \left| \sum_{k=1}^{j-1} \left\{ \left[\left(t_j - t_{k-1}\right)^{1-\alpha} - \left(t_j - t_k\right)^{1-\alpha} \right] \right.\right. \\
&\quad \left.\left. - \left[\left(t_{j-1} - t_{k-1}\right)^{1-\alpha} - \left(t_{j-1} - t_k\right)^{1-\alpha} \right] \right\} D_t^- U_i^k \right| + \frac{t_j - t}{\Gamma(2-\alpha)\left(\triangle t_j\right)^{\alpha}} \left| D_t^- U_i^j \right| \\
&\le \frac{1}{\Gamma(1-\alpha)} \left| \sum_{k=1}^{j-1} \left[\left(\eta_j - t_{k-1}\right)^{-\alpha} - \left(\eta_j - t_k\right)^{-\alpha} \right] \left(t_j - t\right) D_t^- U_i^k \right| + \frac{\left(\triangle t_j\right)^{1-\alpha}}{\Gamma(2-\alpha)} \left| D_t^- U_i^j \right| \\
&\le \frac{\alpha}{\Gamma(1-\alpha)} \left| \sum_{k=1}^{j-1} \left(\eta_j - \vartheta_k\right)^{-\alpha-1} \left(t_j - t\right) \triangle t_k D_t^- U_i^k \right| + \frac{\left(\triangle t_j\right)^{1-\alpha}}{\Gamma(2-\alpha)} \left| D_t^- U_i^j \right| \\
&\le C \max_{1\le k\le j} \left(\triangle t_k\right)^{1-\alpha} \left| D_t^- U_i^k \right|, \qquad (3.8)
\end{aligned}
$$

where $\eta_j \in (t_{j-1}, t_j)$ and $\vartheta_k \in (t_{k-1}, t_k)$. Moreover, we have

$$
\begin{aligned}
\left\| \bar{f}_i(t) - f_i(t) \right\|_{[t_{j-1}, t_j]} &\le \frac{\left(\triangle t_j\right)^2}{2} \sup_{(t_{j-1}, t_j)} \left| f_i''(t) \right| \\
&\le \begin{cases} 0, & 1 \le i \le N-2, \\ C\frac{\left(\triangle t_j\right)^2}{h^2}, & i = N-1. \end{cases} \qquad (3.9)
\end{aligned}
$$

Therefore, combining (3.6) with (3.7)–(3.9) we have

$$
\begin{aligned}
&\left\| L^N \left(\bar{U}_i^K(t) - U_i(t) \right) \right\|_{[0,T]} \\
&\le \begin{cases} C \max\limits_{1\le j\le K} \left(\triangle t_j\right)^{1-\alpha} \left| D_t^- U_i^j \right|, & 1 \le i \le N-2, \\ C \max\limits_{1\le j\le K} \left(\triangle t_j\right)^{1-\alpha} \left| D_t^- U_i^j \right| + C \max\limits_{1\le j\le K} \dfrac{\left(\triangle t_j\right)^2}{h^2}, & i = N-1. \end{cases} \qquad (3.10)
\end{aligned}
$$

Then, the required result of the lemma follows from the semi-discrete stability result (Lemma 3.3) and the inequality (3.10). □

Then the following error estimates for the fully discrete scheme (2.4) can be obtained from Theorems 3.4 and 3.5.

Theorem 3.6. Let $\mathbf{U}(t)$ be the solution vector of the semi-discrete problem (2.3), $\left\{\mathbf{U}^j\right\}_{j=0}^K$ be the numerical solution vector of the fully discrete problem (2.4) and $\bar{U}_i^K(t)$ be the piecewise linear interpolant function of the numerical solution $\left\{U_i^j\right\}_{j=0}^K$ for each i. Then, under the assumption (3.1), the following error estimates

$$
\left\| u(x_i, t) - \bar{U}_i^K(t) \right\|_{[0,T]} \le C \max_{1\le j\le K} \left\{ N^{-2} + \left(\triangle t_j\right)^2 + \left(\triangle t_j\right)^{1-\alpha} \left| D_t^- U_i^j \right| \right\}
$$

for $0 \le i \le N$ hold true, where C is a positive constant independent of the grid.

4. Adapted grid generation

Now, by making use of a posteriori estimates obtained in the above section, we develop an adapted grid for the time discretization. For generating adapted grids a frequently used method is the grid equidistribution method [10, 14, 19]. An adapted grid $\Omega^K \equiv \{0 = t_0 < t_1 < \cdots < t_K = T\}$ can be obtained by using the following grid equidistribution principle [10, 14, 19]

$$\int_{t_{j-1}}^{t_j} M(s)\mathrm{d}s = \frac{1}{K}\int_0^T M(s)\mathrm{d}s, \qquad j = 1, 2, \ldots, K,$$

where $M(t)$ is called the monitor function. Based on a posteriori estimates in Theorem 3.6 we choose the following modified arc-length function

$$\bar{M}(t) = \sqrt{1 + \max_{1\le i<N}\left[\left(\bar{U}_i^K(t)\right)'\right]^2}.$$

as our monitor function. Then we design the following iteration algorithm to generate adapted grids for the time discretization and compute the numerical solutions.

Step 1. Initialize grid: Choose the grid $\Omega^N \times \Omega^{K,(0)}$ as the initial grid, where $\Omega^{K,(0)} = \left\{t_j^{(0)} \mid t_j^{(0)} = jT/K,\ 0 \le j \le K\right\}$.

Step 2. Calculate the discrete solution: Solve the fully discrete problem (2.4) on the grid $\Omega^N \times \Omega^{K,(k)}$ for $U_i^{j,(k)}$, where $\Omega^{K,(k)} = \left\{t_0^{(k)}, t_1^{(k)}, \ldots, t_K^{(k)}\right\}$. Moreover, let

$$l_j^{(k)} = \Delta t_j^{(k)}\sqrt{1 + \max_{1\le i<N}\left(D_t^- U_i^{j,(k)}\right)^2}, \quad I^{(k)} = \sum_{j=1}^{K} l_j^{(k)}.$$

Step 3. Test grid: If

$$\max_{1\le j\le K}\left\{l_j^{(k)}\right\} \le C_0 I^{(k)}/K,$$

holds true for a user-chosen constant $C_0 > 1$, then terminate the iteration and go to Step 5. Otherwise, continuous to Step 4.

Step 4. Make new grid: Generate a new grid $\Omega^{K,(k+1)}$ such that

$$\int_{t_{j-1}^{(k+1)}}^{t_j^{(k+1)}} \sqrt{1 + \max_{1\le i<N}\left[\left(\bar{U}_i^{K,(k)}(t)\right)'\right]^2} = I^{(k)}/K, \qquad j = 1, 2, \cdots, K.$$

Set $k = k + 1$ and go back to step 2.

Step 5. Set $\Omega^{K,*} = \Omega^{K,(k)}$ and $\left\{U_i^{j,*}\right\}_{j=0}^K = \left\{U_i^{j,(k)}\right\}_{j=0}^K$, then stop.

5. Numerical experiments

Two examples are given to indicate experimentally the efficiency and accuracy of the discretization scheme. The comparisons of numerical results on the adapted a posteriori grid and the uniform grid are also given.

Example 5.1. We first consider the following fractional differential equation with a known exact solution as given in [16]:

$$\begin{aligned}
&\frac{\partial^\alpha u}{\partial t^\alpha} - \frac{1}{2}\sigma^2 x^2 \frac{\partial^2 u}{\partial x^2} - (r-q)\, x \frac{\partial u}{\partial x} + ru = f(x,t), && (x,t) \in (0,1) \times (0,1],\\
&u(x,0) = e^x + x + 1, && x \in (0,1),\\
&u(0,t) = t^\alpha + 2, \;\; u(1,t) = t^\alpha + e + 2, && t \in (0,1],
\end{aligned}$$

where $\sigma = 0.1, r = 0.06, q = 0, 0 < \alpha < 1$ and $f(x,t)$ is a function that makes the exact solution satisfying $u(x,t) = t^\alpha + e^x + x + 1$.

Figure 1 shows how a posteriori grid for the time discretization generates by successive iterations of the solution-adapted algorithm for Example 5.1 with $\alpha = 0.2$. The final time grid with $\alpha = 0.2$ is demonstrated in Figure 2. Figures 1 and 2 show that the solution-adapted algorithm automatically refines the grid in a local domain where the exact solution has singular behavior.

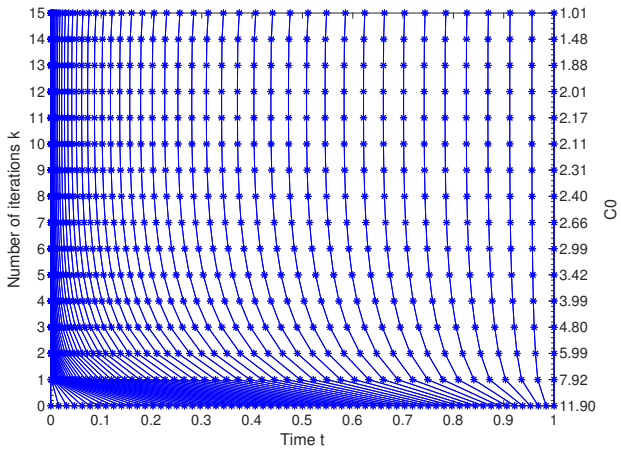

Figure 1. Generation process of the time grid for Example 5.1 with $\alpha = 0.2$.

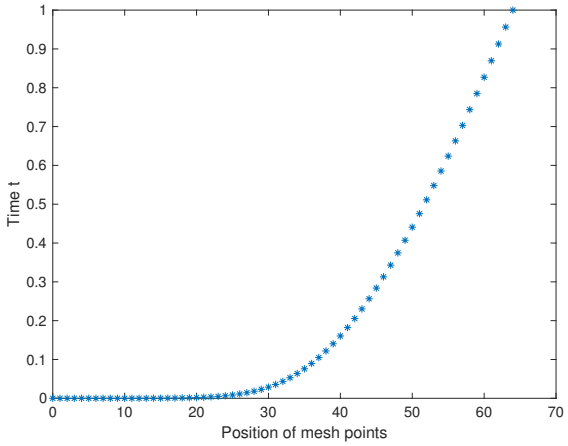

Figure 2. Final time grid for Example 5.1 with $\alpha = 0.2$.

The error in the pointwise maximum norm

$$e^{N,K} = \max_{1\le i\le N, 1\le j\le K} |u_i^j - U_i^j|$$

and the corresponding convergence rate

$$r^N = \log_2(e^{N,K}/e^{2N,2K})$$

are calculated. The errors and convergence rates on a posteriori adapted grid for Example 5.1 are listed in Table 1.

Table 1. Errors in the maximum norm and convergence rates for Example 5.1.

α	grid	Number of grid points $N = K$				
		64	128	256	512	1024
0.2	adapted	4.3606E-3	2.1601E-3	1.1055E-3	5.4408E-4	2.7733E-4
		1.013	0.966	1.023	0.972	-
	uniform	6.2643E-2	5.4541E-2	4.7512E-2	4.1391E-2	3.6056E-2
		0.200	0.199	0.199	0.199	-
0.4	adapted	5.8042E-3	2.7651E-3	1.4079E-3	7.1722E-4	3.6549E-4
		1.070	0.974	0.973	0.973	-
	uniform	3.9175E-2	2.9693E-2	2.2512E-2	1.7067E-2	1.2938E-2
		0.400	0.399	0.399	0.400	-
0.6	adapted	5.1043E-3	2.6002E-3	1.3237E-3	6.7368E-4	3.4284E-4
		0.973	0.974	0.974	0.975	-
	uniform	1.7082E-2	1.1268E-2	7.4347E-3	4.9058E-3	3.2370E-3
		0.600	0.600	0.600	0.600	-
0.8	adapted	4.0806E-3	2.1091E-3	1.0888E-3	5.5982E-4	2.7601E-4
		0.952	0.954	0.960	1.020	-
	uniform	5.8127E-3	3.3318E-3	1.9131E-3	1.0989E-3	6.3119E-4
		0.803	0.800	0.800	0.800	-

Example 5.2. We now consider the following TFBSE without a known exact solution:

$$\begin{aligned}
&\frac{\partial^\alpha u}{\partial t^\alpha} - \frac{1}{2}\sigma^2 x^2 \frac{\partial^2 u}{\partial x^2} - (r-q)\, x \frac{\partial u}{\partial x} + ru = 0, && (x,t) \in (0,X)\times(0,T],\\
&u(x,0) = \max(x-E,0), && x \in (0,X),\\
&u(0,t) = 0, \quad u(X,t) = X - Ee^{-rt}, && t \in (0,T]
\end{aligned}$$

with $\sigma = 0.3, r = 0.06, q = 0.02, E = 10, T = 1, X = 40$ and $0 < \alpha < 1$.

The generation of an adapted a posteriori grid for the time discretization and the final time grid for the TFBSE with $\alpha = 0.2$ are depicted in Figures 3 and 4, respectively. They also show that the solution-adapted algorithm automatically refines the grid in a local domain where the exact solution has singular behavior.

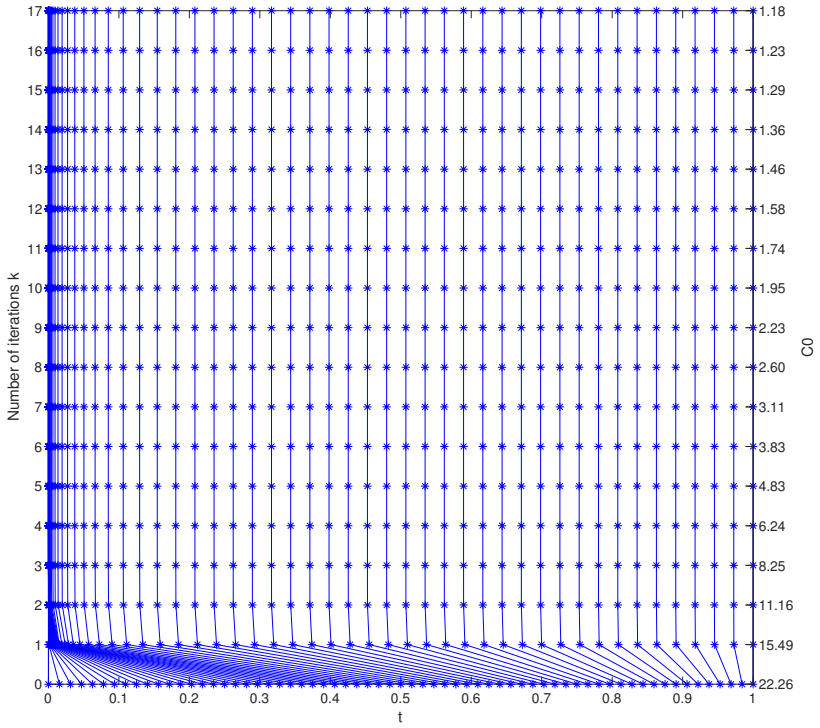

Figure 3. Generation process of the time grid for Example 5.2 with $\alpha = 0.2$.

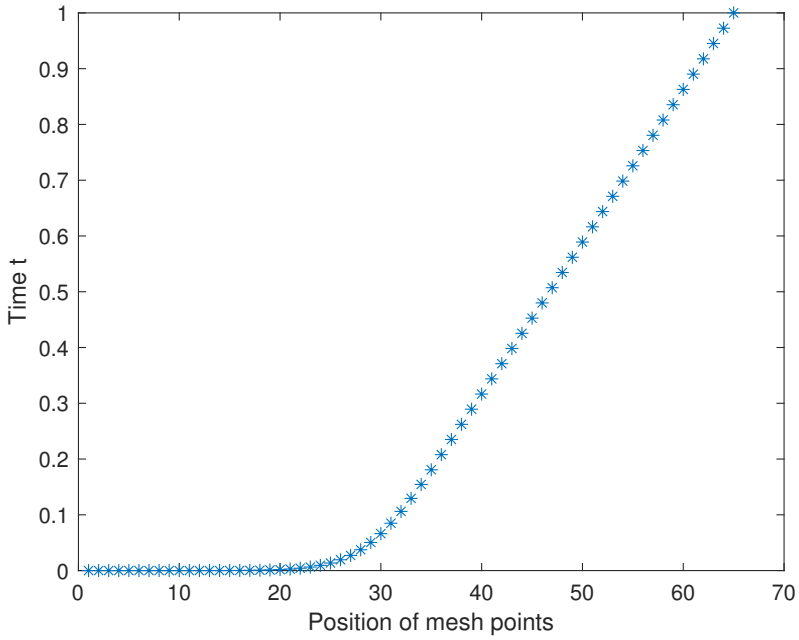

Figure 4. Final time grid for Example 5.2 with $\alpha = 0.2$.

The errors in the pointwise maximum norm and the corresponding experiment convergence rates will be measured based on the double grid principle as follows

$$e^{N,K} = \max_{1\le i\le N, 1\le j\le K} |\bar{U}^{N,K}(x_i, t_j) - \bar{U}^{2N,2K}(x_i, t_j)|$$

and

$$r^N = \log_2(e^{N,K}/e^{2N,2K})$$

respectively, where $\bar{U}^{N,K}(x,t)$ is a linear interpolation of the numerical solution $\left\{U_i^j\right\}$ with spatial discretization parameter N and time discretization parameter K. The errors and convergence rates on a posteriori-adapted grid for Example 5.2 are listed in Table 2.

Table 2. Errors in the maximum norm and convergence rates for Example 5.2.

α	grid	Number of grid points $N = K$				
		6	128	256	512	1024
0.2	adapted	2.4717E-2	1.2288E-2	6.1275E-3	3.0615E-3	1.5314E-3
		1.008	1.004	1.001	0.999	-
	uniform	5.2159E-2	4.1726E-2	3.6868E-2	3.3806E-2	3.1233E-2
		0.179	0.125	0.114	-	
0.4	dapted	2.6537E-2	1.3233E-2	6.6050E-3	3.3000E-3	1.6492E-3
		1.004	1.003	1.001	1.001	-
	uniform	5.4159E-2	3.8341E-2	3.0429E-2	2.5483E-2	2.1785E-2
		0.498	0.333	0.256	0.226	-
0.6	adapted	2.9538E-2	1.4700E-2	7.3761E-3	3.6681E-3	1.8370E-3
		1.007	0.995	1.008	0.998	-
	uniform	4.6999E-2	2.8831E-2	1.9786E-2	1.4805E-2	1.1589E-2
		0.705	0.543	0.418	0.353	-
0.8	adapted	3.1679E-2	1.5729E-2	7.8529E-3	3.9272E-3	1.9572E-3
		1.010	1.002	1.000	1.005	-
	uniform	3.8895E-2	2.1932E-2	1.2798E-2	8.1445E-3	5.6042E-3
		0.827	0.777	0.652	0.539	-

The numerical results in Tables 1 and 2 indicate that the numerical solutions on a posteriori-adapted grids converge to the exact solutions with first-order accuracy in the pointwise maximum error, although the global errors derived in Theorem 3.6 don't reach first-order accuracy. Since the higher-order convergence schemes given in the literature [1, 24] are not suitable for solving the above examples with singular exact solutions, we only give the numerical results of the $L1$ method on the uniform grid as used in [26, 28, 29, 35], which are also presented in Tables 1 and 2. From these results, we verify that our method on an adapted a posteriori grid is more accurate than the method on the uniform grid. Moreover, a posteriori grid scheme can be applied to a broad range of the problems since the generation of adapted grid does not need a priori information of the exact solution, although a posteriori grid scheme proposed in this paper is slightly less accurate than the adapted grid scheme [16] and the variable transformation method [27] based on a priori information of the exact solution.

6. Conclusions and discussion

In this paper, an adapted a posteriori grid method is used to overcome the difficulties caused by the singularity of the exact solution in (1.1). First, the spatial derivatives are discretized by using the central difference method on a piecewise uniform grid. Secondly, the time-fractional derivative is discretized by using the $L1$ approximation method on an arbitrary grid. Thirdly, the stability properties and a posteriori error analysis of the spatial semi-discrete operator are derived. Next, an adapted a posteriori grid for the time discretization is constructed by equidistributing a modified arc-length monitor function based on a posteriori error analysis. Finally, numerical results are given to show that a posteriori-adapted grid fits the singularity of the exact solution well and the $L1$ method with a posteriori-adapted grid is more accurate than the method on the uniform grid. The contribution of this paper is to apply a posteriori grid method to solve the FEBSEs for the first time, which does not need a priori information of the exact solution. In future, we will extend this method to the spatial-fractional Black-Scholes equations and high dimensional fractional Black-Scholes equations whose exact solutions may have singularities.

Acknowledgments

We would like to thank the anonymous reviewers for their valuable suggestions and comments for the improvement of this paper. The work was supported by Zhejiang Province Public Welfare Technology Application Research Project of China (Grant No. LGF22H260003), Zhejiang Provincial Natural Science Foundation of China (Grant No. LTGY23H240002), and Ningbo Municipal Natural Science Foundation (Grant Nos. 2021J178, 2021J179).

Conflict of interest

The authors declare that there is no conflict of interests regarding the publication of this article.

References

1. N. Abdi, H. Aminikhah, A. H. R. Sheikhani, High-order compact finite difference schemes for the time-fractional Black-Scholes model governing European options, *Chaos Soliton. Fract.*, **162** (2022), 112423. http://doi.org/10.1016/j.chaos.2022.112423
2. X. An, F. Liu, M. Zheng, V. V. Anh, I. W. Turner, A space-time spectral method for time-fractional Black-Scholes equation, *Appl. Numer. Math.*, **165** (2021), 152–166. http://doi.org/10.1016/j.apnum.2021.02.009
3. F. Black, M. Scholes, The pricing of options and corporate liabilities, *J. Polit. Econ.*, **81** (1973), 637–654. http://doi.org/10.1086/260062
4. A. Cartea, D. del-Castillo-Negrete, Fractional diffusion models of option prices in markets with jumps, *Physica A*, **374** (2007), 749–763. http://doi.org/10.1016/j.physa.2006.08.071
5. Z. Cen, J. Huang, A. Xu, A. Le, Numerical approximation of a time-fractional Black-Scholes equation, *Comput. Math. Appl.*, **75** (2018), 2874–2887. http://doi.org/10.1016/j.camwa.2018.01.016

6. Z. Cen, A. Le, A robust and accurate finite difference method for a generalized Black-Scholes equation, *J. Comput. Appl. Math.*, **235** (2011), 3728–2733. http://doi.org/10.1016/j.cam.2011.01.018

7. C. Chen, Z. Wang, Y. Yang, A new operator splitting method for American options under fractional Black-Scholes models, *Comput. Math. Appl.*, **77** (2019), 2130–2144. http://doi.org/10.1016/j.camwa.2018.12.007

8. W. Chen, X. Xu, S.-P. Zhu, Analytically pricing double barrier options based on a time-fractional Black-Scholes equation, *Comput. Math. Appl.*, **69** (2015), 1407–1419. http://doi.org/10.1016/j.camwa.2015.03.025

9. P. Das, Comparison of a priori and a posteriori meshes for singularly perturbed nonlinear parameterized problems, *J. Comput. Appl. Math.*, **290** (2015), 16–25. http://doi.org/10.1016/j.cam.2015.04.034

10. P. Das, S. Rana, J. Vigo-Aguiar, Higher order accurate approximations on equidistributed meshes for boundary layer originated mixed type reaction diffusion systems with multiple scale nature, *Appl. Numer. Math.*, **148** (2020), 79–97. https://doi.org/10.1016/j.apnum.2019.08.028

11. A. Farhadi, M. Salehi, G. H. Erjaee, A new version of Black-Scholes equation presented by time-fractional derivative, *Iran. J. Sci. Technol. Trans. Sci.*, **42** (2018), 2159–2166. https://doi.org/10.1007/s40995-017-0244-7

12. A. Golbabai, O. Nikan, A computational method based on the moving least-squares approach for pricing double barrier options in a time-fractional Black-Scholes model, *Comput. Econ.*, **55** (2020), 119–141. https://doi.org/10.1007/s10614-019-09880-4

13. A. Golbabai, O. Nikan, T. Nikazad, Numerical analysis of time fractional Black-Scholes European option pricing model arising in financial market, *Comput. Appl. Math.*, **38** (2019), 173. https://doi.org/10.1007/s40314-019-0957-7

14. S. Gowrisankar, S. Natesan, An efficient robust numerical method for singularly perturbed Burgers' equation, *Appl. Math. Comput.*, **346** (2019), 385–394. https://doi.org/10.1016/j.amc.2018.10.049

15. S. Haq, M. Hussain, Selection of shape parameter in radial basis functions for solution of time-fractional Black-Scholes models, *Appl. Math. Comput.*, **335** (2018), 248–263. https://doi.org/10.1016/j.amc.2018.04.045

16. J. Huang, Z. Cen, J. Zhao, An adaptive moving mesh method for a time-fractional Black-Scholes equation, *Adv. Differ. Equ.*, **2019** (2019), 516. https://doi.org/10.1186/s13662-019-2453-1

17. G. Jumarie, Derivation and solutions of some fractional Black-Scholes equations in coarse-grained space and time. Application to Merton's optimal portfolio, *Comput. Math. Appl.*, **59** (2010), 1142–1164. https://doi.org/10.1016/j.camwa.2009.05.015

18. M. N. Koleva, L. G. Vulkov, Numerical solution of time-fractional Black-Scholes equation, *Comput. Appl. Math.*, **36** (2017), 1699–1715. https://doi.org/10.1007/s40314-016-0330-z

19. N. Kopteva, N. Madden, M. Stynes, Grid equidistribution for reaction-diffusion problems in one dimension, *Numer. Algor.*, **40** (2005), 305–322. https://doi.org/10.1007/s11075-005-7079-6

20. L.-B. Liu, Y. Chen, Maximum norm a posteriori error estimates for a singularly perturbed differential difference equation with small delay, *Appl. Math. Comput.*, **227** (2014), 801–810. https://doi.org/10.1016/j.amc.2013.10.085

21. L.-B. Liu, Y. Chen, A-posteriori error estimation in maximum norm for a strongly coupled system of two singularly perturbed convection-diffusion problems, *J. Comput. Appl. Math.*, **313** (2017), 152–167. https://doi.org/10.1016/j.cam.2016.08.020

22. Y. Luchko, Maximum principle for the generalized time-fractional diffusion equation, *J. Math. Anal. Appl.*, **351** (2009), 218–223. https://doi.org/10.1016/j.jmaa.2008.10.018

23. R. C. Merton, Theory of rational option pricing, *Bell J. Econ. Manag. Sci.*, **4** (1973), 141–183. https://doi.org/10.2307/3003143

24. S. M. Nuugulu, F. Gideon, K. C. Patidar, A robust numerical scheme for a time-fractional Black-Scholes partial differential equation describing stock exchange dynamics, *Chaos Soliton. Fract.*, **145** (2021), 110753. https://doi.org/10.1016/j.chaos.2021.110753

25. A. Pedas, E. Tamme, Piecewise polynomial collocation for linear boundary value problems of fractional differential equations, *J. Comput. Appl. Math.*, **236** (2012), 3349–3359. https://doi.org/10.1016/j.cam.2012.03.002

26. P. Roul, V. M. K. P. Goura, A compact finite difference scheme for fractional Black-Scholes option pricing model, *Appl. Numer. Math.*, **166** (2021), 40–60. https://doi.org/10.1016/j.apnum.2021.03.017

27. M. She, L. Li, R. Tang, D. Li, A novel numerical scheme for a time fractional Black-Scholes equation, *J. Appl. Math. Comput.*, **66** (2021), 853–870. https://doi.org/10.1007/s12190-020-01467-9

28. L. Song, W. Wang, Solution of the fractional Black-Scholes option pricing model by finite difference method, *Abstr. Appl. Anal.*, **2013** (2013), 194286. https://doi.org/10.1155/2013/194286

29. R. H. De Staelen, A. S. Hendy, Numerically pricing double barrier options in a time-fractional Black-Scholes model, *Comput. Math. Appl.*, **74** (2017), 1166–1175. https://doi.org/10.1016/j.camwa.2017.06.005

30. M. Stynes, J. L. Gracia, A finite difference method for a two-point boundary value problem with a Caputo fractional derivative, *IMA J. Numer. Anal.*, **35** (2015), 689–721. https://doi.org/10.1093/imanum/dru011

31. M. Stynes, E. O'Riordan, J. L. Gracia, Error analysis of a finite difference method on graded meshes for a time-fractional diffusion equation, *SIAM J. Numer. Anal.*, **55** (2017), 1057–1079. https://doi.org/10.1137/16M1082329

32. Z. Tian, S. Zhai, H. Ji, Z. Weng, A compact quadratic spline collocation method for the time-fractional Black-Scholes model, *J. Appl. Math. Comput.*, **66** (2021), 327–350. https://doi.org/10.1007/s12190-020-01439-z

33. P. Wilmott, J. Dewynne, S. Howison, *Option pricing: mathematical models and computation*, Oxford, UK: Oxford Financial Press, 1993.

34. W. Wyss, The fractional Black-Scholes equations, *Fract. Calc. Appl. Anal.*, **3** (2000), 51–61.

35. H. Zhang, F. Liu, I. Turner, S. Chen, The numerical simulation of the tempered fractional Black-Scholes equation for European double barrier option, *Appl. Math. Model.*, **40** (2016), 5819–5834. https://doi.org/10.1016/j.apm.2016.01.027

36. H. Zhang, F. Liu, I. Turner, Q. Yang, Numerical solution of the time fractional Black-Scholes model governing European options, *Comput. Math. Appl.*, **71** (2016), 1772–1783. https://doi.org/10.1016/j.camwa.2016.02.007

AIMS Press